Phase Shifted Pulse Height Modulated Motor Control for Multiply Actuated Joints to Optimize Operating Characteristics

Submitted: 18th December 2015; accepted: 19th May 2016

Torsten Siedel, Stefan Bethge, Manfred Hild

DOI: 10.14313/JAMRIS_2-2016/12

Abstract:

In this article, we propose two model free control schemes that are based on pulse height modulation using low frequencies with the goal to compensate normal friction effects in drive trains that negatively influence the performance of e.g. a standard PID controller. The first control scheme uses pulse height modulation to especially compensate stick slip effects but increases vibration and noise in the drive train. To reduce such side effects a modified phase shifted pulse height control scheme based on multiple actuated joints is introduced. Both control schemes are compared with a standard linear controller as reference and evaluated by using six quality criteria.

Keywords: *Multiple Actuators, Model-free, Friction Compensation, Pulse Modulation*

1. Introduction

In many actuation applications, motors are combined with a gearbox to change transmission. This increases friction effects and leads to a notable reduction in control quality when using conventional controllers like PID control. Effects such as delayed response and non-linear control torque relationships can especially be observed when using low rotational speeds or when driving high loads.

Various compensation methods have been proposed that attempt to create friction models to predict the actual friction of the system and improve motor controllers based on them. Le-Tien and Albu-Schäffer [4] use a static friction model describing Coulomb, viscose and load dependent friction. Olsen et. al. [7] investigate the behaviors of the dynamic Lu-Gre and Bliman-Sorine friction models to derive compensation methods and show results from practical experiments. Swevers et. al. [12] extend these models by incorporating hysteresis with non-local memory and achieve improved accuracy in compensation.

Usually, parameters for both static or dynamic models have to be adapted to each controlled system separately and this can prove to be cumbersome. Consequently, parameter identification methods [14] or adaptive compensation through learning such as neural networks [9] or adaptive fuzzy systems have been proposed [13].

Instead of using active compensation, different model-free methods have been investigated that reduce friction outside of the controller. Well known techniques include dither [17], [8] and pulsed motor control [15], [16]. Dither is the introduction of a high-frequency noise signal into non-linear systems in order to help the system stabilize. It is employed successfully in hydraulic and pneumatic use cases while it has some detrimental properties when used with direct-drive actuators.

Pulsed or impulsive motor control is a method that reduces the system's stiction by pulsing the motor control with pulses large enough to overcome stiction only when the motor is in low speeds. This is especially useful when starting and stopping often and operating with low rotation speeds, as is usually the case in robotics applications. The optimal length and amplitude of the pulses depend on the system properties. Appropriate methods to obtain them are discussed e.g. in [15].

Drawbacks of both methods adding artificial oscillation to the system are possible noise and higher wear of mechanic components. By using multiply actuated joints, some of these can be alleviated through combined control upon the behavior of pulsed control with only one motor. Multiply actuated joints are also employed e.g. in robotics to achieve regulated joint stiffness [1]. Further benefits are increased efficiency, redundancy and fail-safety [3], [11], [2].

In this article we employ an adapted pulse based motor control method to reduce friction effects. To reduce the disadvantageous side-effects of those methods, namely vibration and noise, we propose a novel control method based on the use of multiple parallel actuators for one joint and emphasize its properties in reducing those effects. In the following, two variations of motor control methods for multiple actuators are compared with a standard linear controller as reference. The behavior of a motor unit is evaluated by means of six quality criteria. The described control methods are closely related to results given in Siedel [10] which focuses on the methods applied for robotic purposes. Various figures are also taken from there.

2. Multiply Actuated Motor Unit

The motor unit employs multiple identical actuators for which the servo unit Dynamixel RX-28 by ROBOTIS was used. In this article, only the use of identical actuators is investigated. Further options can also be gained by combining actuators with different gain ratios and output powers, cf. [6]. The unit consists of a DC motor, a spur gear and electrical components for motor drive, communication and control. The DC motor is an RE-max 17 from Maxon (see [5] for specifica-

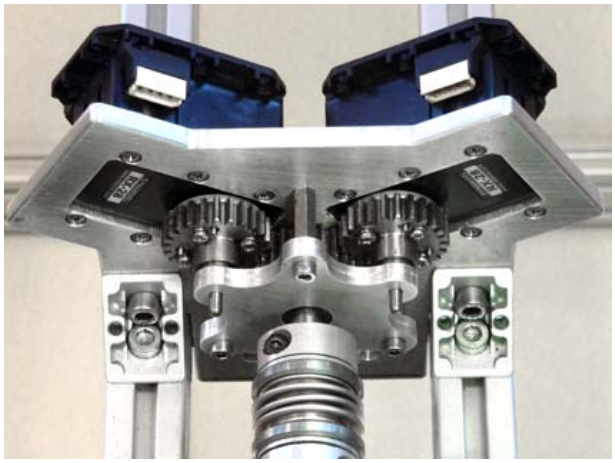

Fig. 1. The coupling gearbox with two RX-28s. The servo units are coupled to the measuring shaft with the spur gear. The lower part of the picture shows the measuring shaft that is coupled to the attached measuring devices using a balancer coupling

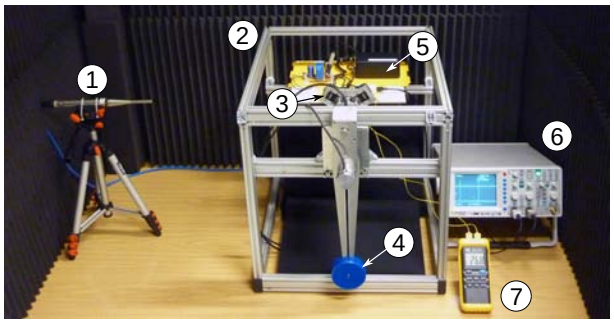

Fig. 2. Test setup enclosed in sound isolating foam panels. Left: Measuring microphone (1) at 0.5 ***m distance to the motor unit. Middle: drive test bench (2) with motor unit (3), pendulum (4) and control electronics (5). Right: Two-channel oscilloscope (6) and temperature sensor (7)***

tions) and is operating on 12 to 16 V. An STMicroelectronics L6201 H-bridge is used as the power driver for the motor. On the low level, the motor is driven with a pulse width modulated voltage at a frequency of 15.6 kHz. The five-stage spur gear has a gear ratio of 1:195. With the exception of the output socket gear that is mounted on double ball bearing, all gears are mounted on plain bearing. In the motor unit, two motors are coupled directly with the measuring shaft at a ratio of 1:1, see Figure 1. The whole drive train – servo gearbox and coupling – has a backlash of 0.8 degrees.

3. Experimental Setup

The center of Figure 2 shows the drive test bench which contains the motor unit with two servo units, a torque sensor that is rotationally decoupled and an optical angle sensor. The sensors are assembled in a coaxial manner, preventing the introduction of additional mechanical backlash. A microcontroller board with an STM32 processor is used for motor control and data communication to and from a connected computer.

Attached to the end of the measuring shaft is a pendulum with the following properties:

- mass $m_\mathrm{P} = 1168\,\mathrm{g}$
- length $l_\mathrm{P} = 0.282\,\mathrm{m}$
- rotatory inertia $J_\mathrm{P} = 99\,\mathrm{gm}^2$

The pendulum mass and lever arm length are chosen in such a way that the maximum drive torque is not sufficient to deflect the pendulum to the horizontal plane at slow speeds. This also avoids overshoot.

Figure 2 also shows additional measuring devices which are used to evaluate the drive characteristics based on the previously defined quality criteria. A HAMEG HM1008-2 digital oscilloscope measures motor current and voltage to get the motor power consumption while an RS-components digital thermometer gets the current motor temperature. Since the oscilloscope uses discrete sampling, an LC filter is added. The temperature readings are only used to maintain comparable starting conditions for each test run and are not recorded. An HDM M30 measurement microphone is placed in a 50 cm distance to provide sound pressure measurements. The whole setup is enclosed by special acoustic foam panels to reduce ambient noise and to improve the sound measurement quality.

3.1. Test Sequence

All of the following experiments are carried out under uniform conditions regarding motor temperature, operating voltage and ambient noise. Each test takes 20 seconds. The actuators are controlled without any feedback.

Tests are started with the pendulum hanging down so that no torque is applied to either measurement shaft or the motor unit. Over the first 10 seconds the motor reference voltage U_ref for both motors is gradually increased from 0 V up to 14.8 V which raises the pendulum in one direction. During the next 10 seconds the power is gradually decreased down to 0 V again so the pendulum is lowered again. The progression of the reference voltage can be seen in the upper part of Figure 3.

The duration of 20 seconds for each test is chosen so that the motors do not heat up considerably and at the same time dynamical effects can be disregarded because of rather slow raising and lowering of the pendulum. To minimize the influence of measurement scattering, each test is repeated five times and the values are averaged over all five runs.

4. Reference Control

The first test is intended to show the current situation with gearbox induced friction effects and will serve as reference measurement. For readability, the vector

$$U(t) = \begin{pmatrix} U_1(t) \\ U_2(t) \end{pmatrix} \tag{1}$$

is the combined vector of the voltages of both motors $U_1(t)$ and $U_2(t)$. For the reference measurement, both

servos get the same voltage signal,

$$U_1(t) = U_2(t) = U_{\mathrm{ref}}(t) \tag{2}$$

so both motors always apply the same torque. The lower part of Figure 3 displays the movement (or trajectory) of the pendulum for each of the five tests. The single test trajectories as well as the averaged trajectory over all tests both show extensive non-linearities and hysteresis effects. These are caused by friction in the gearboxes of both servo units.

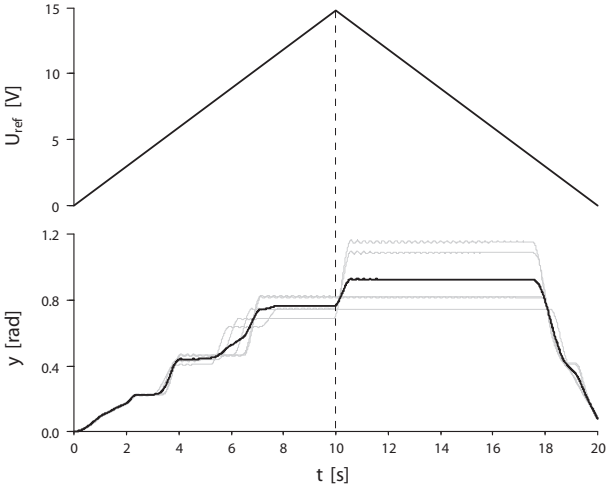

Fig. 3. Top: reference voltage U_{ref} sweep over time. Bottom: single trajectories of the pendulum (grey lines) resulting from the reference voltage from subsequent trials and averaged trajectory (black). The dashed line labels the turning point of the reference voltage

In the first half of the test runs, the influence of the well known stick-slip effect is clearly visible, which raises the pendulum with stuttering motion. Following the law of Coulomb, both friction types are proportional to the motor drive torque. This leads to the observation that the relation between the static friction and the dry friction is independent of the applied torque. With the static friction coefficient μ_{S} and the dry friction coefficient μ_{D},

$$\frac{\mu_{\mathrm{S}}}{\mu_{\mathrm{D}}} = \text{constant.} \tag{3}$$

Also see [4] for more details on torque dependent friction effects.

As dynamic effects can be neglected, it is possible to compare the start and end of each plateau of the rising trajectory and conclude on the difference of the friction coefficients. Starting with the dry friction coefficient μ_{D}, it can be seen that in this test case the sticky friction is 38.8 % stronger than the dry friction (with a standard deviation of 12.8 %). The driving torque therefore has to be increased by 38.8 % to further lift the pendulum after it came to a standstill. In general, this value is greatly dependent on the type of gearbox and the ratio of transmission but also on various other factors such as lubrication, operating temperature and wear.

The topmost plateau marks the maximum angle the pendulum has reached in that particular test run. This area is shifted forward on the time axis, while some jumps are even happening only after the maximum voltage has been reached at 10 seconds. The difference between the maximum angle that the pendulum reaches in single runs is up to 0.41 rad. Until reaching the maximum reference voltage U_{ref} the whole drive train is in drive mode. Drive mode is here used to name one of the modes of four quadrant operation of servo motors. In drive mode, motor torque and turning direction are the same whereas in brake mode, the directions are opposing each other. The motor moment is acting in the turning direction and the friction torque is acting against the motor torque, in effect reducing the effective torque. When the reference voltage is decreased, the motor moment is also reduced without changing the motor direction. The pendulum should be lowering. The motor unit however is now in brake mode, so motor torque and friction torque are adding up. The pendulum is also not moving since static friction is still effective which is larger than dry friction. As a result, the pendulum is only lowering after the driving voltage falls short of 22.2 % of the maximum reference voltage. The pendulum then starts suddenly and is moving quickly in the beginning.

This test using conventional control shows which non-linear and hysteretic effects can occur in the drive unit. These effects are of course also dependent on the parameters of the pendulum and the behavior of the reference voltage.

5. Pulse Height Modulated Motor Control

In order to mitigate these effects, a common technique is to use pulsating motor drive rather than continuous motor drive [15], allowing the motor to always move even for very small target values. Usually pulse width modulated (PWM) drive is used which alters the duty cycle to achieve the desired drive voltage on average. Using the similar pulse height modulated (PHM) motor control which changes the height of equally distributed pulses has the benefit of a much higher possible resolution when the temporal resolution of the digital circuitry in use is not very high. The basic idea of these techniques is to change between the friction types (stiction and dry friction) as well as the motor modes (drive and brake mode) in a controlled manner with comparably low frequency in order to linearize the drive behavior.

First, the operation of the PHM drive will be described. It is implemented in three steps: creating the base oscillation, modifying the oscillation amplitude in relation to the reference voltage and combining the reference voltage with the oscillation. The base oscillation is derived from an analytic representation of the triangle oscillation

$$f_{\Delta}(x) = \frac{2}{\pi}\,\sin^{-1}\big(\sin(2\,\pi\,x)\big)\,. \tag{4}$$

which is modified to alter the amplitude as necessary. The triangle oscillation $f_{\Delta}(x)$ is expanded with the parameters a_{B} to alter the amplitude, and f_{B} to alter the

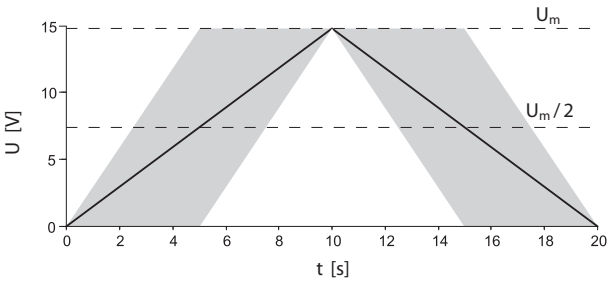

Fig. 4. Envelope curve (grey) of the modulated oscillation in relation to the reference signal U_{ref} ***(black line). The dashed lines indicate half of the maximum voltage and effective maximum voltage*** $U_{\max}$ ***(***14.8 ***V).***

frequency

$$U_{\mathrm{B}}(t) = a_{\mathrm{B}}\, f_{\Delta}(f_{\mathrm{B}}\, t) \tag{5}$$

with t being the time variable to receive the base frequency voltage $U_{\mathrm{B}}(t)$. The amplitude a_{B} of the base frequency is modified in relation to the reference voltage within a range of 0 to $U_{\max}/2$ V. A reference voltage of $U_{\mathrm{ref}} = 0.00\,\mathrm{V}$ relates to an amplitude of 0.00 V while $U_{\mathrm{ref}} = U_{\max}/2$ relates to an amplitude of $U_{\max}/2$. When the reference voltage assumes values greater than $U_{\max}/2$ up to $U_{\max}$, the amplitude is falling down to 0.00 V to not receive values above the maximum drive voltage. Figure 4 shows the reference voltage (black) and the envelope of the pulse modulated voltage (grey) as it is set in the later test runs.

The amplitude progression in relation to the reference voltage can be given as

$$a_{\mathrm{B}} = \begin{cases} 2\,U_{\mathrm{ref}} & \text{at } \frac{-U_{\mathrm{m}}}{2} \le U_{\mathrm{ref}} \le \frac{U_{\mathrm{m}}}{2} \\ 2\,U_{\mathrm{m}} - 2\,U_{\mathrm{ref}} & \text{at } U_{\mathrm{ref}} < \frac{-U_{\mathrm{m}}}{2} \wedge U_{\mathrm{ref}} > \frac{U_{\mathrm{m}}}{2} \end{cases} \tag{6}$$

Finally, the amplitude modulated base oscillation is added to the reference voltage and the resulting signal is passed to both motors similarly.

$$U_1(t) = U_2(t) = U_{\mathrm{ref}}(t) + U_{\mathrm{B}}(t) \tag{7}$$

In order to determine which pulse frequency delivers closest to ideal behavior, five different frequencies for the base oscillation were tested. The frequencies were chosen with regard to the frequency of the motor control loop which is working with 100 Hz. Accordingly, the highest possible frequency is 50 Hz of which 25 Hz, 12.5 Hz, 6.25 Hz and 3.125 Hz are derived.

As mentioned, each frequency test run is repeated five times and averaged. The obtained trajectories are displayed in Figure 5 which also includes the trajectories from the previous test (reference control) for comparison.

Comparing the results of the reference control, all PMC trajectories more or less display the following properties: The spread of the trajectories is lower, a plateau forms at higher values of the reference voltage and the stick-slip effect is minimized as can be seen in as smooth motion in place of the previous jumps and

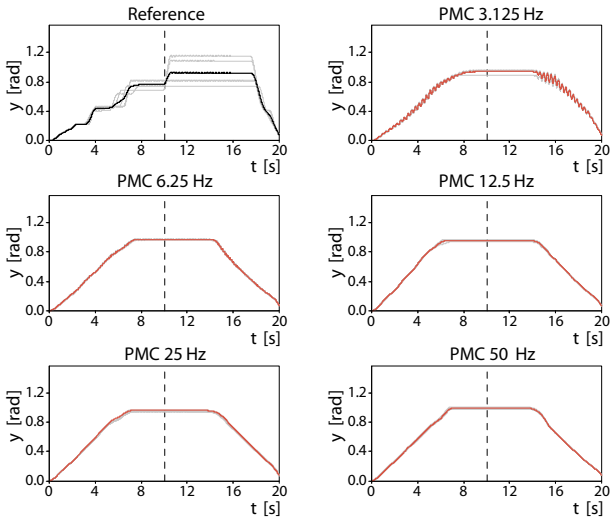

Fig. 5. Trajectories of the pendulum with reference control and with PMC at five different base frequencies (3.125 ***Hz to*** 50 ***Hz). The separate trajectories are drawn in grey, the averages for each frequency in red. The black line shows the averaged trajectory for the reference control***

stuttering. Finally, the hysteresis is greatly reduced and the trajectory is closer to being symmetrical.

At 3.125 Hz, influence of the frequency is clearly visible as a modulated frequency during upwards and downwards motion. Higher frequencies don't produce this behavior anymore as the pendulum's inertia acts as a low pass filter that removes higher frequencies. The frequencies from 6.25 Hz to 50 Hz do not produce significant differences between the trajectories, suggesting low influence of the specific frequency.

6. Phase Shifted Pulse Height Modulated Motor Control

A possible modification of the previously described PMC is to have each motor be pulsed at different points in time with phase shifted modulated pulse oscillations. In the case of two motors, the signals are shifted by π, phase shift for any other number of motors will be looked at in the next section. The expanded equation

$$U_{\mathrm{B}}(t) = a_{\mathrm{B}}\, f_{\Delta}(f_{\mathrm{B}}\, t + \varphi) \tag{8}$$

yields a phase shifted oscillation with φ as the phase shift parameter. Using $\varphi_1 = 0$ and $\varphi_2 = \pi$ for φ, the base oscillations $U_{\mathrm{B}_1}(t)$ and $U_{\mathrm{B}_2}(t)$ are obtained and, written as a vector

$$U(t) = \begin{pmatrix} U_{\mathrm{ref}}(t) + U_{\mathrm{B}_1}(t) \\ U_{\mathrm{ref}}(t) + U_{\mathrm{B}_2}(t) \end{pmatrix}, \tag{9}$$

are fed to both the motors. With this altered control method, again five test runs per base frequency are performed. The resulting trajectories are shown in Figure 6 which again includes the resulting trajectories of the reference control test for comparison.

At the lowest frequency of 3.125 Hz, the pendulum is raised almost continuously to just before reaching

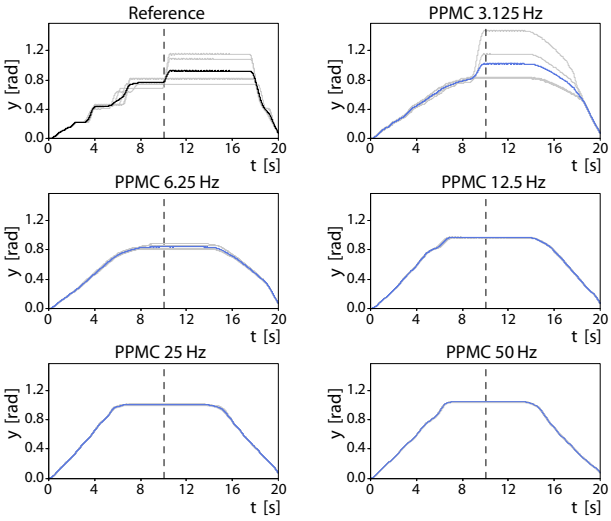

Fig. 6. Trajectories of the pendulum with reference control and with PPMC at five different base frequencies (3.125 Hz to 50 Hz). The separate trajectories are drawn in grey, the averages for each frequency in red. The black line shows the averaged trajectory for the reference control

the maximum voltage. Then the results are scattered. The plateaus of all five trajectories are more or less of the same length but clearly shifted forward on the time axis, showing the influence of the motor drive modes. At a frequency of 6.25 Hz no jumps in the trajectories are visible anymore, but the transitions to the plateaus are more smooth. As with the PMC, the PPMC shows only marginal differences at higher frequencies (12.5 Hz, 25 Hz and 50 Hz)

7. Results

The visual examination of the trajectories only allows limited conclusions about the properties of the particular control methods, of which PMC and PPMC also show frequency dependent behavior. Apart from the movement alone shown by the trajectory of the pendulum, other quality measures are important to judge each control method appropriately. These include the torque behavior, energy consumption, hysteresis, linearity, maximum torque, operating smoothness, energy efficiency and operational noise. These can either be measured directly or derived from the taken measures trajectory, torque, energy consumption and operating noise. A significance analysis was made to make sure that, regarding the standard deviation over the repeated measurements, the best results are significantly better. The results of the best and second best test run within each quality measure are tested for significant difference with a two-sample t-test. The chosen significance criterion for difference is $p > 5\%$.

7.1. Hysteresis

Starting with determining the hysteresis, we look at the trajectory. In the present case, the hysteresis describes the difference of the trajectory when increasing ($t = 0$ to 10 seconds) and decreasing ($t = 10$ to 20 seconds) height. The quality is determined as follows: first, the second half of the trajectory is mirrored at the middle axis (at 10 seconds) onto the first half. The diagrams that are produced in this way are shown in Figure 7. The direction of movement is labelled with arrows. It is well visible how much ascent and descent overlap and therefore exhibit a certain hysteresis.

A numerical value for the hysteresis is obtained as the sum of the squared errors. The corresponding equation is

$$E_{\mathrm{H}}(y) = \sum_{t=0}^{T/4} \big(y(t) - y(T/2 - t)\big)^2 \qquad (10)$$

where the error is assumed as the vertical distance between the ascent and descent curves for each time step.

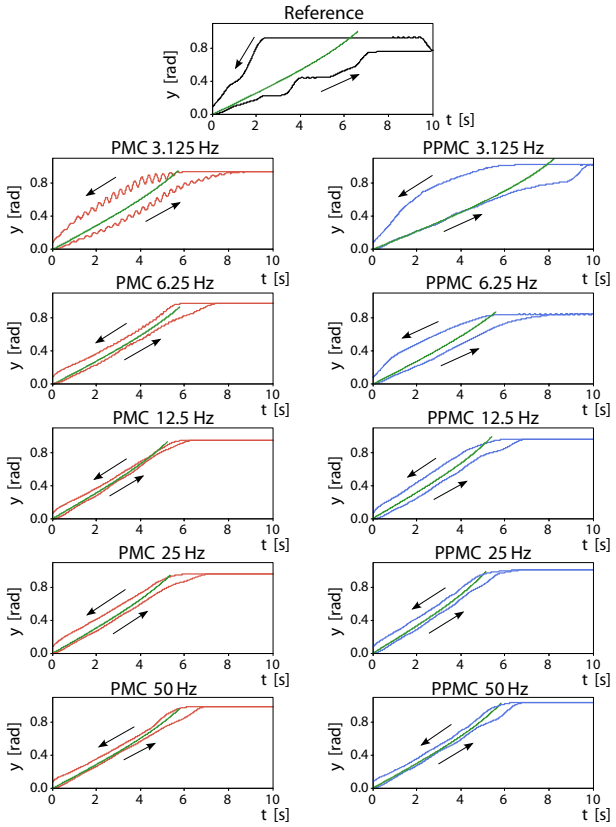

Fig. 7. Comparison between hysteresis and linearity of averaged trajectories. The individual graphs show ascent and descent of averaged trajectories with the different control methods. The direction of motion is labeled with arrows while the additional curves between the trajectories show the ideal course of the respective trajectory assuming no friction. It is computed using a motor model, using parameters derived from the actual trajectories

A good result for the hysteresis is achieved if E_{H} is minimal and therefore the area between rising and falling trajectory is as small as possible. The best result was measured for the PMC at 12.5 Hz. Comparing to the second best result, the PPMC at 12.5 Hz, the best result is significantly better.

7.2. Linearity

The next step is to evaluate the linearity of the trajectory, which covers the extent to which the drive behavior influenced by the real friction approaches the ideal friction free behavior. To evaluate the drive characteristics we have another look at the individual pendulum trajectories. In order to picture an ideal trajectory graph, the physical properties of the pendulum and a simple DC servo motor model is employed which assumes a directly proportional relation between motor current and torque and ignores friction or dynamical effects. Except for the torque constant, all parameters for the model are known. The actual operating behavior is heavily dependent on the control method used (Reference, PMC and PPMC) which is why the torque constant has to be determined for each test run separately. This is done with the least squares method. The resulting ideal trajectories based on the model are adjusted to the real trajectories. Since the upper plateaus of the trajectories are distorting the values, only the data up to 90 % of the maximum angle are used. The determined ideal trajectories can be seen in Figure 7 between the trajectories of ascent and descent.

For these areas of each measurement, it is now possible to get the linearity deviation of the averaged real course $\overline{y_\mathrm{r}}$ to the ideal course y_i. This is done again by computing the sum of squared errors.

$$E_\mathrm{L} = \sum_{t=0}^{T_{10\,\%}} \left(\overline{y_\mathrm{r}}(t) - y_\mathrm{i}(t)\right)^2. \qquad (11)$$

A positive result for Linearity is achieved if E_L is small. The best result was obtained for the PMC at 6.25 Hz which is significant in comparison to the PPMC at 6.25 Hz.

7.3. Maximum Torque and Vibrations

For assessing the torque behavior of the motor unit we look at the effective torque that is measured with the torque sensor between drive train and the pendulum. The quality of the behavior is determined by the criteria maximum torque and occurring vibrations. The maximum torque that can be delivered is determined by averaging the torque values around the point at which the pendulum is at maximum height. Averaging is done, as the dynamic behavior of the pendulum might result in high torque values for a short time which however can not be maintained over longer time spans. The best result for maximum torque was achieved for the PPMC at 50 Hz which is significantly better in comparison to the PMC at 50 Hz.

Vibrations are on the one hand produced by oscillations resulting from the sticky friction in the gearbox but on the other hand because of the pulsated control signal. Figure 8 shows exemplary torque measurements for trajectories for each control method. The reference control on the left shows vibrations because of the alternating friction types. The PMC however shows vibrations resulting from the pulsed control.

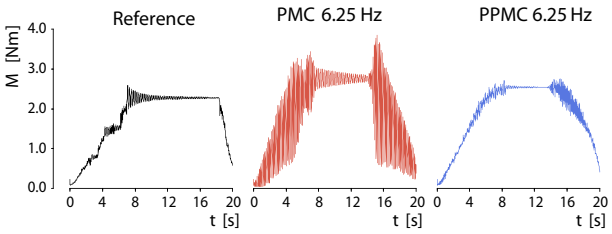

Fig. 8. Exemplary effective torque courses for three different control methods. Left: Reference, Middle: PMC (6.25 Hz), Right: PPMC (6.25 Hz)

Using the same base frequency, the PPMC shows noticeably less vibrations because of phase shifted control of both motor units where pulses can compensate for each other inside of the coupling gear.

The vibrations can be quantized by fast Fourier-transforming (FFT) the torque signal, yielding a frequency spectrum for each torque signal. The value of the frequency with the maximum overall level is assumed as the vibration level. The best result for vibrations was achieved for the PPMC at 25 Hz which is significantly better in comparison to the PMC at 25 Hz.

7.4. Energy Consumption

For the energy consumption, the measurements for current and voltage are used which are obtained using the oscilloscope. Figure 9 shows exemplary data for the power consumption for each of the control methods. Reference control and PPMC produce similar curves. Only in the middle of ascent and descent, small fluctuations are visible. However, when using PMC, noticeable fluctuations are produced that have the same height as the amplitude of the oscillation that is modulated onto the reference voltage U_ref.

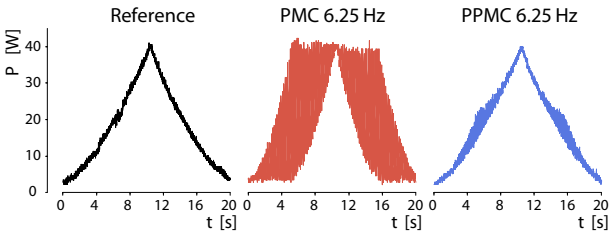

Fig. 9. Exemplary power consumption courses for three different control methods. Left: Reference, Middle: PMC (6.25 Hz), Right: PPMC (6.25 Hz)

Regarding the energy consumption, no immediate disadvantage is to be expected from the fluctuations, as long as the input power is not exceeding the control electronics. Crucial to the quality of the control method rather is the overall energy usage of the actuators per trial run, determined by the time integral

$$E_\mathrm{A} = \int_0^T U(t)\, I(t)\, dt \qquad (12)$$

of the product of operating voltage $U(t)$, current $I(t)$ and T being the duration of the test run. Smaller values of E_A are better. The best result was achieved with the

reference control which is significant in comparison to the PMC and PPMC at all frequencies.

7.5. Operating Noise

The sound produced is measured at a sample rate of 48 kHz (mono) to evaluate the control method quality. As before for vibrations, a frequency analysis is done and the level of the maximal frequency is obtained as an indicator for the amount of noise generated.

Here, the best result was obtained for the PMC at 3.125 Hz which is significant in comparison to the PPMC at 3.125 Hz.

7.6. Overall Rating

Summarizing the results for each of the criteria, the values are normalized and mapped to a color range and arranged in an overview matrix as seen in Figure 10. Each result is marked by color and additionally an "x" or "o" to show if it is above or below average. The best result for each criterion is marked with a white triangle.

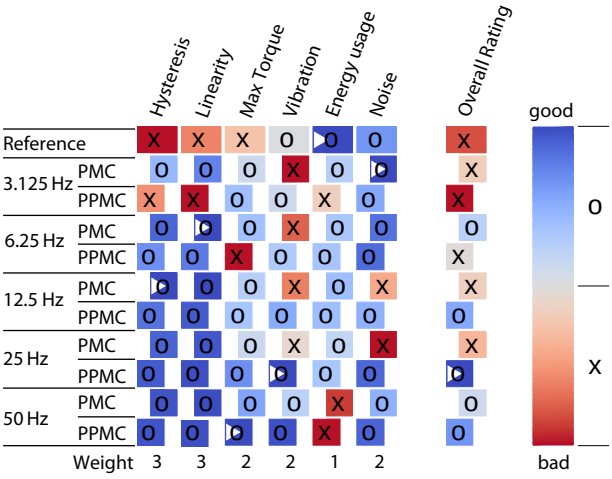

Fig. 10. Color coded rating matrix for the three control methods Reference, PMC and PPMC by means of the quality criteria Hysteresis, Linearity, Maximum Torque, Vibration, Energy Consumption and Noise Generation (column 1 to 6). Column 7 displays the average value over the criteria and gives an overall rating for the individual control method. The chosen weights relate to the influence each criterion has for the overall rating (3: strong, 2: medium and 1: low). White triangles mark the best result for each criterion

While determining the quality criteria, it was noticed that the results for each criterion have different variance, i.e. the differences between best and worst result vary. Also, the results show that each criterion does not have the same importance for the evaluation. Therefore three different steps of weighting were introduced (see Figure 10). The overall results on the right side show a weighted sum of quality criteria.

It is noteworthy that the best results are not distributed equally. None of the rows – meaning none of the control methods – achieves more than one best result. The same can be said for the worst results. The best overall result is produced with the PPMC at 25 Hz. This control method shows the best single value in vibration behavior and overall good values for the other criteria. The next best result is the PPMC at 50 Hz and the worst after the reference control is the PPMC at 3.125 Hz.

In conclusion, the PPMC shows the benefits of multiple actuators and the possibilities of thereby enhanced control methods. The improvement of the overall drive behavior is considerable compared to the conventional reference control method. The only disadvantage, albeit small, is the energy consumption that is about 3 % higher for PPMC at 25 Hz.

8. PPMC Conversion for an Arbitrary Amount of Coupled Actuators

In order to expand the PPMC to more than two actuators, the phase shift φ_i for all motors has to be distributed equally to the whole cycle duration of the control signal, aiming for minimal vibration and noise generation. The same principle applies to combustion engines, where the succession of the ignition for each cylinder is equally distributed to one turn of the crank shaft.

Since discrete signal processing does not allow every desired phase shift, the distribution has to be aligned to what is possible. In the following method, odd or even amounts of actuators are dealt with separately.

8.1. Even Number of Actuators

As described in Section 6 the base oscillation for the second motor is being shifted by π, so that both compensate for the torque impulses of the other. To keep this principle for more motors, the phase shifts over the first half of the cycle duration ($0 \leq \varphi < \pi$) have to be identical to those over the second half ($\pi \leq \varphi < 2\,\pi$). Furthermore, to reach as even a distribution as possible of all phase shifts over the cycle duration in order to minimize vibrations and noise, the PPMC for N actuators is adjusted as follows.

In the beginning, the amount of work cycles of the control circuitry during one period of the base oscillation is determined. The amount Z_B is

$$Z_\mathrm{B} = \frac{f_\mathrm{C}}{f_\mathrm{B}}\,, \tag{13}$$

where f_C is the working frequency of the control circuitry and f_B is the frequency of the base oscillation.

A possible base oscillation with frequency f_B for the PPMC following Section 6 necessitates that Z_B is even. Otherwise the maxima of the base oscillation could be lost in the discretized representation.

Since the amount N of actuators is not necessarily a multiple of Z_B, it has to be determined which subdivisions of Z_B are possible. For that, let W be the set of even dividers of Z_B as defined by

$$W := \{\mathrm{x} \in \mathbb{N} \mid x \text{ divides } Z_\mathrm{B} \ \wedge \ x \text{ even}\}\,. \tag{14}$$

The set is only allowed to contain even dividers as otherwise an equal distribution of the actuators across

both half periods would not be possible. In the following, W will be regarded as a set that is sorted in descending order, where W_i is the i'th element of that set and z is the number of elements of W, $z = |W|$. Since Z_B is even in any case, the last element of W is

$$W_z = 2\,. \tag{15}$$

For better illustration, the elements of W can also be understood as layers where the i'th layer W_i contains subdivisions of the cycle duration. Figure 11 displays an exemplary phase shift matrix with the possible phase shifts W_i for each layer drawn as rectangles. The amount of actuators that is resulting from the subdivisions is then listed in each of the rectangles.

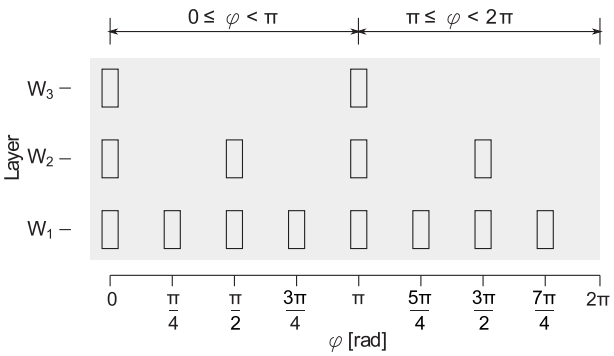

Fig. 11. Exemplary phase shift matrix for the values: $Z_\mathrm{B} = 8$ ***and*** $W = \{8,\ 4,\ 2\}$***. The rectangles indicate the possible phase shifts***

It is now possible for each subdivision or layer W_i to determine how many sets of actuators q_i it can hold. The amount of actuators for each layer is

$$N_i = q_i W_i\,. \tag{16}$$

In order to keep the difference between the phase shifts and thereby the temporal distance between the power peaks as small as possible, the actuators are assigned to the layers of the matrix in ascending order, i. e. the lowest layer with the finest time grid is always filled first. The following scheme is used:

$$\begin{aligned} q_1 &= \left\lfloor \frac{N}{W_1} \right\rfloor \\ q_2 &= \left\lfloor \frac{N - N_1}{W_2} \right\rfloor \\ q_3 &= \left\lfloor \frac{N - N_1 - N_2}{W_3} \right\rfloor \\ &\vdots \\ q_z &= \left(\frac{N - \sum_{i=1}^{z-1} N_i}{W_z} \right) \end{aligned} \tag{17}$$

It therefore has to hold true that

$$N = N_1 + N_2 + N_3 + \cdots + N_z\,. \tag{18}$$

The distribution of the actuators is now given. For that we have to determine the associated phase shifts. We first get the step size of the phase shifts

$$\Delta\varphi_i = \frac{2\,\pi}{W_i} \tag{19}$$

in relation to the i'th layer, whereas the cycle duration is normalized to $2\,\pi$. In total, there are N_i actuators, let $k_i \in \{1,\ \ldots,\ N_i\}$. The phase shift $\varphi^i_{k_i}$ assigned to the step size $\Delta\varphi_i$ for the k'th actuator can be determined for all actuators by

$$\varphi^i_{k_i} = ((k_i - 1) \bmod W_i)\,\Delta\varphi_i\,. \tag{20}$$

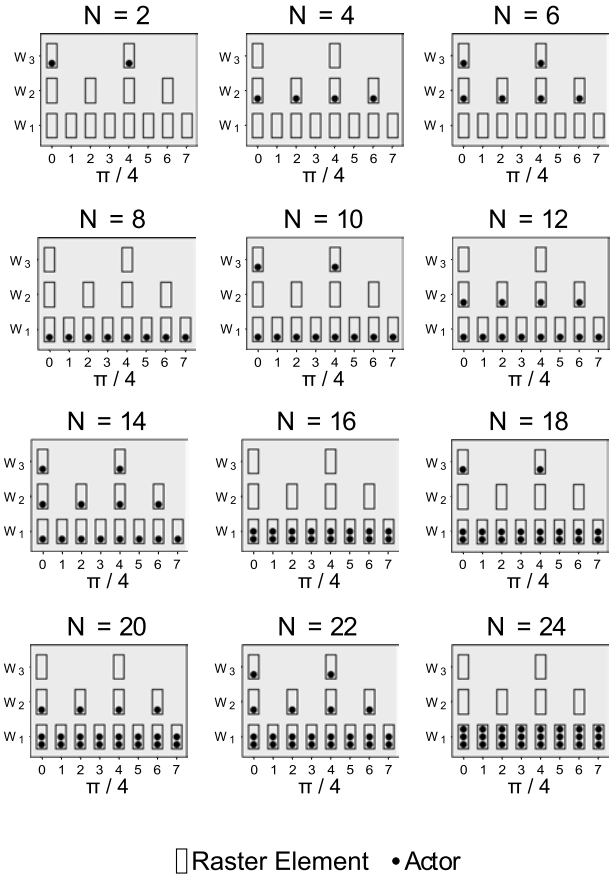

Fig. 12. Distribution of the actuators in a phase shift matrix that is generated from $Z_\mathrm{B} = 8$***. Solely an even amount of actuators*** $N = \{2,\ 4,\ \ldots,\ 24\}$ ***is used***

This method obtains the phase shift values for an arbitrary even amount of actuators and examples can be seen in Figure 12. All actuators can be distributed equally on the lowest layer of the matrix (W_1). Because of the high pulse frequencies possible, the lowest vibrations are expected. Furthermore, the power maxima are always at the same level if all actuators are put on the same level of the matrix which should have a positive influence on the operating smoothness.

8.2. Uneven Number of Actuators

With the intent to evenly distribute the phase shifts over both halves $0 \le \varphi < \pi$ and $\pi \le \varphi < 2\,\pi$ of the cycle duration of the control voltage, the distribution

for an odd number of actuators can not be symmetrical. This can also be checked with equation 18. If it is however necessary to use an uneven amount of actuators, the phase shift for an actuator can be determined using

$$\varphi_N = \left(\frac{Z_\mathrm{B}}{2} - 1\right) \frac{2\,\pi}{W_1} \tag{21}$$

and

$$\varphi_N = (Z_\mathrm{B} - 1)\,\frac{2\,\pi}{W_1}\,. \tag{22}$$

That way it is at least ensured that for the according points in time the torque load of inside the drive train is minimal in the case that the other actuators can not be distributed solely on the lowest layer and therefore the maximum torques are unequal. The calculation of the phase shift values for the remaining actuators $N-1$ can be done following the method as described before. It is to be noted that when using an uneven amount of actuators, the asymmetry has less of an effect the more actuators are used.

9. Conclusion

The present article has pointed out some of the gearbox induced friction effects that occur when two actuators and a conventional control method are used. The effects are resulting from sticky friction and dry friction (producing among others the stick-slip effect), and effects that are based on the differences between the effective torque of the two motor operating modes (drive mode and brake mode) and the associated hysteresis of the drive behavior. In order to compensate for those effects, first a modified variant of classic pulse modulated control (PMC) was examined. It showed typical side-effects such as increased vibration and noise. Based upon the PMC, the novel phase shifted pulse modulated control (PPMC) was introduced. The PPMC is derived from the PMC and leverages the possibilities of multiple actuators to improve on the PMC.

After presenting the experimental setup and the test procedure, the trajectories of the test load (pendulum) that are resulting from the individual test runs for the control methods reference control, PMC and PPMC have been discussed. Only looking at the trajectories gives first clues to the benefits of using either PMC or PPMC over the reference method. A detailed evaluation of the control quality was given in subsequent sections based on the six quality criteria energy consumption, hysteresis, linearity, maximum torque, operating smoothness, energy efficiency and operational noise. The various properties of the control methods were then compared.

To produce comparable results, the tests used two coupled standard DC servomotors (Dynamixel RX-28) in all cases. The separate comparison results as well as the overall ratings showed that the PPMC at a base frequency of 25 Hz has the best overall result, where it delivered good to very good results for all criteria. The typical hysteresis effects from the conventional control method can be compensated almost completely and the linearity could be improved noticeably. Moreover, because of the phase shifted control of both motors, the PPMC exhibits significantly less vibration and noise generation compared to the PMC. The only measured disadvantage is the slightly increased energy consumption that is 3 % higher than the unpulsed control method.

Subsequently it has been described how the PPMC can be generalized to drive trains with an arbitrary amount of parallel actuators. For this, each servo unit needs its own phase shifted modulated pulse signal controlling the motor in succession to the others. With the obtained distribution of the phase shifts, a low-noise and low-vibration operation is ensured.

Both operating methods PMC and PPMC are especially well suited for slow movements. When increasing the speed of movement, the influence of the stick-slip effect to hysteresis is decreasing. Switching between pulsed and unpulsed controllers is possible to rely on the properties on other control methods.

AUTHORS

Torsten Siedel – Space Applications Services NV/SA, Leuvensesteenweg 325, 1932 Zaventem, Belgium, e-mail: torsten.siedel@spaceapplications.com.

Stefan Bethge – Department of Advanced Robotics, Istituto Italiano di Tecnologia, Via Morego 30, 16163 Genoa, Italy, e-mail: stefan.bethge@iit.it.

Manfred Hild – Neurorobotics Research Laboratory, Beuth-Hochschule für Technik Berlin, e-mail: hild@beuth-hochschule.de, www: http://neurorobotics.eu/.

REFERENCES

[1] M. G. Catalano, G. Grioli, M. Garabini, F. Bonomo, M. Mancinit, N. Tsagarakis, and A. Bicchi, "VSA-CubeBot: a Modular Variable Stiffness Platform for Multiple Degrees of Freedom Robots". In: *International Conference on Robotics and Automation (ICRA)*, 2011, 5090 – 5095.

[2] J. Davies, R. Dixon, R. M. Goodall, and T. Steffen, "Multi-agent Control of High Redundancy Actuation", *International Journal of Automation and Computing*, vol. 11, no. 1, 2014, 1 – 9.

[3] R. Dixon, T. Steffen, J. Davies, A. Zolotas, J. Pearson, and X. Du, "HRA-Intrinsically Fault Tolerant Actuation Through High Redundancy", 2009.

[4] L. Le-Tien and A. Albu-Schäffer, "Adaptive Friction Compensation in Trajectory Tracking Control of DLR Medical Robots with Elastic Joints". In: *International Conference on Intelligent Robots and Systems (IROS)*, 2012.

[5] Maxon Motor AG. *Datasheet, RE-max 17*, April 2012.

[6] J. B. Morrell and J. K. Salisbury, "Parallel-Coupled Micro-Macro Actuators", *The International Journal of Robotics Research*, 1998.

[7] H. Olsson, K. J. Åström, C. Canudas de Wit, M. Gäfvert, and P. Lischinsky, "Friction Models and Friction Compensation", *European Journal of Control*, vol. 4, 1998, 176 – 195.

[8] A. A. Pervozvanski and C. Canudas-De-Wit, "Asymptotic analysis of the dither effect in systems with friction", *Automatica*, vol. 38, no. 1, 2002, 105–113.

[9] R. R. Selmic and F. L. Lewis, "Neural-network approximation of piecewise continuous functions: application to friction compensation", *Neural Networks, IEEE Transactions on*, vol. 13, no. 3, 2002, 745–751.

[10] M. T. Siedel. *Hybride Steuerung parallel gekoppelter Aktoren am Beispiel des humanoiden Roboters Myon*. PhD thesis, Institut für Informatik, Humboldt-Universität zu Berlin, 2015.

[11] T. Steffen, R. Dixon, R. M. Goodall, and A. Zolotas. "Requirements Analysis for High Redundancy Actuation". Technical report, Department of Electronic and Electric Engineering, Loughborough University, 2007.

[12] J. Swevers, F. Al-Bender, C. Ganseman, and T. Projogo, "An integrated friction model structure with improved presliding behavior for accurate friction compensation", *Automatic Control, IEEE Transactions on*, vol. 45, no. 4, 2000, 675–686.

[13] Y. Wang, D. Wang, and T. Chai, "Extraction and adaptation of fuzzy rules for friction modeling and control compensation", *Fuzzy Systems, IEEE Transactions on*, vol. 19, no. 4, 2011, 682–693.

[14] Z. Wenjing, "Parameter identification of lugre friction model in servo system based on improved particle swarm optimization algorithm". In: *Control Conference, 2007. CCC 2007. Chinese*, 2007, 135–139.

[15] T. Wescott. "Controlling Motors in the Presence of Friction and Backlash". http://www.wescottdesign.com/, 2010. [Online; retrieved March 8th, 2013].

[16] T. M. Yang Sangsik, "Adaptive pulse width control for precise positioning under the influence of stiction and coulomb friction.", *ASME Journal of Dynamical Systems, Measurement and Control*, vol. 110, 1988, 221–227.

[17] G. Zames and N. A. Shneydor, "Dither in nonlinear systems", *IEEE Transactions on Automatic Control*, vol. 21, no. 5, 1976, 660––667.